ACS APPLIED MATERIALS & INTERFACES

Research Article

Cite This: ACS Appl. Mater. Interfaces 2019, 11, 10328−10336

www.acsami.org

Self-Healing Four-Dimensional Printing with an Ultraviolet Curable Double-Network Shape Memory Polymer System

Biao Zhang,[†,‡] Wang Zhang,[†,§] Zhiqian Zhang,[∥] Yuan-Fang Zhang,[†] Hardik Hingorani,[†] Zhuangjian Liu,[∥] Jun Liu,[∥] and Qi Ge*[,†,§]

[†]Digital Manufacturing and Design Center and [§]Science and Math Cluster, Singapore University of Technology and Design, 487372, Singapore

[‡]Shaanxi Institute of Flexible Electronics (SIFE) & Xi'an Institute of Biomedical Materials and Engineering (IBME), Northwestern Polytechnical University (NPU), 710072 Xi'an, China

[∥]Institute of High Performance Computing (IHPC), A*STAR, 138632 Singapore, Singapore

Supporting Information

ABSTRACT: Four-dimensional (4D) printing that enables 3D printed structures to change configurations over time has gained great attention because of its exciting potential in various applications. Among all the 4D printing materials, shape memory polymers (SMPs) possess higher stiffness and faster response rate and therefore are considered as one of most promising materials for 4D printing. However, most of the SMP-based 4D printing materials are (meth)acrylate thermosets which have permanently cross-linked covalent networks and cannot be repaired if any damage occurs. To address the unrepairable nature of SMP-based 4D printing materials, this paper reports a double-network self-healing SMP (SH-SMP) system for high-resolution self-healing 4D printing. In the SH-SMP system, the semicrystalline linear polymer polycaprolactone (PCL) is incorporated into a methacrylate-based SMP system which has good compatibility with the digital light processing-based 3D printing technology and can be used to fabricate complex 4D printing structures with high resolution (up to 30 μm). The PCL linear polymer imparts the self-healing ability to the 4D printing structures, and the mechanical properties of a damaged structure can be recovered to more than 90% after adding more than 20 wt % of PCL into the SH-SMP system. We investigated the effects of PCL concentration on the thermomechanical behavior, viscosity, and the self-healing capability of the SH-SMP system and performed the computational fluid dynamics simulations to study the effect of SH-SMP solution's viscosity on the 3D printing process. Finally, we demonstrated the self-healing 4D printing application examples to show the merits of the SH-SMP system.

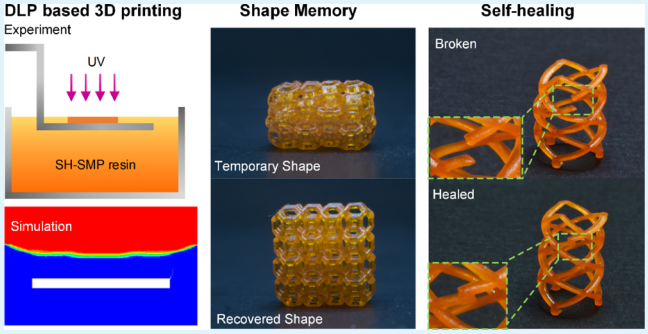

KEYWORDS: *self-healing, shape memory polymer, 4D printing, DLP-based 3D printing, semicrystalline polymer*

1. INTRODUCTION

Four-dimensional (4D) printing, a technology that adds the fourth dimension "time" into 3D printed geometries,[1−5] has gained great attention because of its exciting potential in the fields of soft robotics,[6,7] medical devices,[8,9] flexible electronics,[10] and many others.[4,11−13] This technology is realized by printing 3D geometries with soft active materials (SAMs) that can actively transform configurations in a predefined manner over time in response to external stimuli.[4,5,8,12−14]

So far, the SAMs that have been widely used in 4D printing fall into two classes: hydrogels[3,4,11,15] and shape memory polymers (SMPs).[8,9,16,17] A variety of hydrogel-based 4D printing including biomimetic 4D printing,[4] active valves,[18,19] complex self-evolving structures,[3] and others[20−22] have been achieved. However, the low-material stiffness (from ∼1 to ∼100 kPa)[4,18] and slow response rates in the time scale from tens of minutes to a few hours[3,4,23] limit the further application of hydrogel-based 4D printing.[3,4,23] In contrast, SMPs which enable the fixation of a temporary shape and the recovery to the permanent shape upon environmental stimuli, such as heat,[24,25] light,[26−28] or electrical field,[29,30] possess higher stiffness (from ∼MPa to ∼GPa[24,25]) and fast response rates to realize shape recovery in seconds.[31,32] Because of these superior properties, SMP-based 4D printing has been widely used in the fields of actuators, biomedical devices, and many others.[12,13] Most of these reported SMP-based 4D printing examples were realized by 3D printing structures with (meth)acrylate-based monomers and cross-linkers,[1−3,8,33] which form permanently cross-linked covalent networks that attribute the capability of "memorizing" the original shapes of

Received: January 7, 2019
Accepted: February 20, 2019
Published: February 20, 2019

DOI: 10.1021/acsami.9b00359
ACS Appl. Mater. Interfaces 2019, 11, 10328−10336

the 3D printed structures. However, once these covalent networks are damaged, the damaged printed structures are not repairable and can only be discarded, which causes extra material cost and environmental burden. Therefore, it is needed to develop new 4D printing materials with self-healing property which can be repaired and reused in the case that 4D printing structures are damaged.

To date, there are only two papers that report the methods to develop self-healing SMP (SH-SMP)-based 4D printing materials. Kuang et al. developed a self-healing and shape memory (SM) elastomer for 4D printing.[17] They realized such self-healing 4D printing by developing a 3D printing ink that contains urethane diacrylate and linear semicrystalline polymer. Nevertheless, because of the high viscosity, the developed ink is only suitable to the UV-light-assisted direct ink write (DIW) 3D printing technology. The way of directly writing 3D structures by extruding the printing ink through the printing nozzle with ∼100 μm diameter significantly limits the resolution and geometrical complexity of printed 3D structures. Different from the DIW 3D printing technology, the digital light processing (DLP)-based 3D printing is able to realize fast fabrication of complex 3D structures with feature size ranging from 1 to 100 μm by employing the digital mask projection to trigger the localized photopolymerization.[8,34,35] Recently, Invernizzi et al. developed a self-healing 4D printing SMP that is suitable to the DLP-based 3D printing.[36] SM and self-healing functionalities are thermally triggered and obtained, respectively, using polycaprolactone (PCL) chains and 2-ureido-4[1*H*]-pyrimidinone units co-cross-linked in a polymer system. However, a healed sample can only recover ∼50% of its original tensile strength and ∼20% of its original failure strain. More importantly, this work did not fully exploit the advantage of DLP-based 3D printing and only demonstrated simple 2D printed samples.

In this article, we present a method to prepare SH-SMPs for high-resolution 4D printing. In the developed SH-SMP system, benzyl methacrylate (BMA) and poly(ethylene glycol)-dimethacrylate (PEGDMA), respectively, serve as the linear chain builder and cross-linker to form a highly deformable and 3D printable SMP network, and polycaprolactone (PCL) is incorporated into the network system as a self-healing agent to provide self-healing properties to the 4D-printed structures. The SH-SMP has good compatibility with DLP-based 3D printing which enables the fabrication of complex 4D printing structures with high resolution (up to 30 μm). The PCL linear polymer imparts the self-healing ability to the 4D printing structures, and the mechanical properties of a damaged structure can be recovered to more than 90%. The development of SH-SMPs will extend the lifespans of high-resolution 4D printing structures and be beneficial to a variety of practical 4D-printing-related applications including soft robotics,[37−39] aerospace structures,[40,41] biomedical devices,[42,43] and others.[12,13]

2. MATERIALS AND METHODS

2.1. Procurement of Materials and Chemicals. All of the material constituents that form the SH-SMP including BMA, PEGDMA (Mn = 550 g/mol), and PCL pellets (Mn ≈ 80 000 g/mol) were purchased from Sigma-Aldrich and used as received. Other chemicals including diphenyl(2,4,6-trimethylbenzoyl)phosphine oxide (TPO) as a photoinitiator and Sudan I as a photoabsorber for the DLP-based 3D printing as well as dichloromethane as a solvent were also purchased from Sigma-Aldrich and used as received.

2.2. Solution Preparation. We prepared the SH-SMP 3D printing polymer solution by first mixing 75 g of BMA with 25 g of PEGDMA. Then, PCL pellets were added into the obtained BMA−PEGDMA mixtures at 70 °C until the solution became transparent. The weight concentration of PCL, C_{PCL}, is defined as $m_{PCL}/(m_{BMA} + m_{PEGDMA}) \times 100\%$, where m_{PCL}, m_{BMA}, and m_{PEGDMA} are the weights of PCL, BMA, and PEGDMA, respectively. When we prepared the SH-SMP solution with C_{PCL} higher than 30 wt %, dichloromethane with the same weight as PCL was added to the SH-SMP solution to reduce the viscosity. The photoinitiator TPO (5 wt % of the total weight of BMA and PEGDMA) and the photoabsorber Sudan I (0.02−0.5 wt % of the total solution weight) were added to the SH-SMP solution at room temperature. Dichloromethane was evaporated by using a vacuum oven until the weight became constant.

2.3. 3D Printing Process. We printed the self-healing 3D structures on a self-built high-resolution 3D printing platform with the prepared SH-SMP polymer solution. Details about the 3D printing platform and the printing process can be found in our previous report.[8] The printing parameters are presented in Table S1. After printing, the printed structures were rinsed in a cleaning solution with 80 vol % of isopropanol and 20 vol % of dichloromethane to remove the unpolymerized SH-SMP solution. Finally, the printed structures were postcured in a UV oven (365 nm, UVP, Ultraviolet Crosslinkers, Upland, CA, USA) for 10 min.

2.4. Dynamic Mechanical Analysis. We conducted the dynamic mechanical analysis (DMA) to investigate the thermomechanical behaviors of the printed SH-SMP samples. The tests were conducted on a DMA tester (TA Instruments, Q800 DMA, U.S.) in the tension film mode at a frequency of 1 Hz and an amplitude of 10 μm. The force track mode with 125% was used to adjust the static force that follows the stiffness change of the tested sample during temperature ramps. After erasing thermal history at 80 °C for 10 min, DMA tests started from −80 to 120 °C at a heating rate of 2 °C/min. The dimensions of the testing samples were 25 mm × 5 mm × 0.6 mm. Each composition was tested at least two times to ensure a good repeatability.

2.5. Uniaxial Tensile Experiments. We performed the uniaxial tensile tests to characterize the Young's modulus of the SH-SMP samples at room and higher temperatures. For the room-temperature tests, they were conducted on a uniaxial tensile tester (Instron, model 5943, Germany) with a 1 kN load cell. The dimensions of the testing samples were 20 mm × 10 mm × 0.5 mm. For higher temperature tests (at 90 °C), they were performed on the DMA tester, and the dimensions of the testing samples were 25 mm × 5 mm × 0.6 mm. The testing strain rate was 1%/s. The Young's modulus of a tested sample was identified as the initial slope of the material stress−strain curve in the linear regime.

2.6. Differential Scanning Calorimetry Experiments. We conducted differential scanning calorimetry (DSC) experiments to investigate the melting and crystallization behaviors of PCL in the SH-SMP system. The tests were performed on a DSC instrument (TA Instruments, model DSC Q20A, U.S.) equipped with a refrigerated cooling system. After equilibrating the samples at −85 °C for 5 min, the first heating trace started from −85 to 120 °C at 10 °C/min. The samples were equilibrated at 120 °C for 1 min and then cooled down at 3 °C/min. When the temperature arrived at −90 °C, the samples were equilibrated for 1 min and finally heated again to 120 °C at 10 °C/min. The first cooling and second heating traces were recorded to study the melting and crystallization behaviors of PCL. Each composition was tested at least three times to ensure a good repeatability.

2.7. SM Behavior Characterizations. We investigated the SM behavior of the SH-SMP samples by following the typical SM cycling method. The sample was first stretched by 10% with a constant strain rate of 6%/min at a programming temperature (i.e., T_{trans} + 30 °C; T_{trans}: transition temperature of a specific tested SH-SMP sample). Then, the temperature was decreased to 25 °C at a cooling rate of 2 °C/min. After reaching the targeted programming temperature, the sample was held isothermally for 2 min. The strain of the temporary shape was measured after removing the external load. In the free

DOI: 10.1021/acsami.9b00359
ACS Appl. Mater. Interfaces 2019, 11, 10328−10336

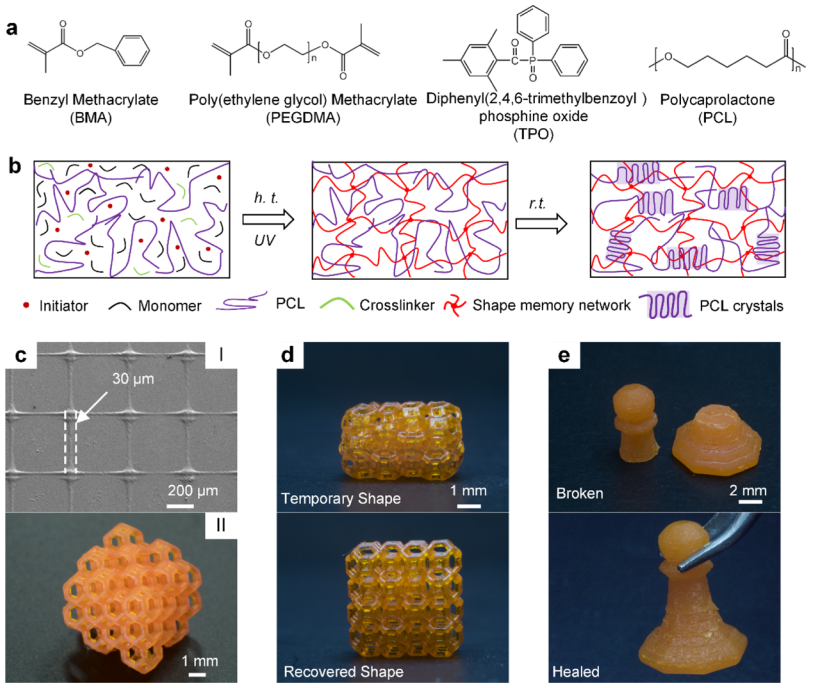

Figure 1. Schematic illustrations of DLP-based 3D printing using SH-SMPs. (a) Chemical structures of the components in SH-SMP solution. (b) Chemical structure evolution of the SH-SMP solution during UV-based 3D printing at high temperature (h.t.) and cooling down to room temperature (r.t.). (c) High-resolution complex 3D structures printed using SH-SMP solution. (I) 3D printed high-resolution grid; (II) 3D printed Kelvin foam; (d) demonstration of 4D printing: temporary shape (top) and permanent shape (down) of 3D printed Kelvin foam; and (e) demonstration of the self-healing ability of the printed 3D structure: the broken chess piece (top) can be healed together (down) by heating at 80 °C for 5 min.

recovery step, the temperature was gradually increased to the recovery temperature (i.e., T_{trans} + 30 °C) at the rate of 2 °C/min. The sample was held isothermally for another 60 min to observe the free recovery behavior. The SM behavior characterizations were performed on the DMA tester. The dimensions of the testing samples were 25 mm × 5 mm × 0.6 mm.

2.8. Lap Shear Experiments. We studied the self-healing ability of the printed SH-SMP samples following the procedures of a standard lap-shear test.[44] The experiments were carried out on the uniaxial tensile tester (Instron, model 5943, Germany) with a 1 kN load cell. The lap shear specimens were prepared by attaching two rectangular samples (width × thickness = 10 mm× 1.5 mm) with the shear area of 7 mm × 10 mm using a Mohr clamp in an oven at 80 °C for 30 min to ensure full bonding between two samples. The control specimens with the same dimensions and shear area were prepared by 3D printing. Then, the tensile tests were performed on the assembly at a speed of 1%/s. Each composition was tested at least three times for repeatability.

2.9. Rheological Characterizations. We performed the rheological characterizations to investigate the temperature-dependent viscosity of the SH-SMP solution. The tests were conducted on a Discovery Hybrid Rheometer (DHR2, TA instruments Inc., UK) with an aluminum plate geometry (40 mm in diameter). The tests were conducted with frequency ranging from 0.1 to 100 Hz. SH-SMP solutions with each composition were tested from 25 to 115 °C with an increment of 10 °C. The temperature was precisely controlled by a Peltier system. The plate gap was set as 500 μm.

2.10. Goniometer Measurements. We measured the surface tension and contact angle to obtain the related parameters that were later used in the computational fluid dynamic (CFD) simulations of the 3D printing processes with SH-SMP solutions. The measurements were carried out on an optical contact angle and interface tension meter (SL200KS, KINO, USA). The solutions with 0.1% Sudan I were held by a 1 mL syringe with a 1.8 mm outer diameter needle. Then, the surface tension between 3D printing solution and air was measured by the pendant drop method, and the contact angle between solution droplet and the printing platform was measured by fitting the contour of the solution droplet on a plate made of the same material (VeroBlack, Stratasys, USA) as the printing platform.

2.11. Scanning Electron Microscopy. We used scanning electron microscopy (SEM) to analyze the microstructure of the samples. SEM images were acquired on Hitachi SU8010 SEM (Hitachi Ltd., Chiyoda, Tokyo, Japan). The samples were attached to a SEM holder and then gold-sputtered in vacuum before the test.

3. RESULTS AND DISCUSSION

In this article, we report a self-healing 4D printing double-network SMP system by incorporating a semicrystalline linear polymer as a healing agent into a methacrylate-based SMP which has been successfully used in high-resolution 4D printing.[8] Figure 1a presents the detailed chemicals that are used for preparing the UV curable solution that forms self-healing 4D printing structures. In the solution, BMA, PEGDMA, and TPO work as a monomer, cross-linker, and photoinitiator, respectively, for photopolymerizing the methacrylate-based SMP network; PCL is chosen as the semicrystalline healing agent. We choose PCL as the healing agent because of its excellent miscibility with the methacrylate-based SMP system and relatively low melting temperature (about 60 °C). Other thermoplastics with the two abovementioned properties can also be considered to be used as the healing agent. The printing solution is prepared by mixing all the chemicals at a temperature which is higher than the melting temperature (T_m) of the healing agent. Details about the solution preparation are provided in Section 2.2.

As depicted in Figure 1b, we start the printing process by heating the solution above the T_m of PCL, followed by irradiating patterned UV images onto the SH-SMP solution. The UV image triggers the localized photopolymerization that

DOI: 10.1021/acsami.9b00359
ACS Appl. Mater. Interfaces 2019, 11, 10328−10336

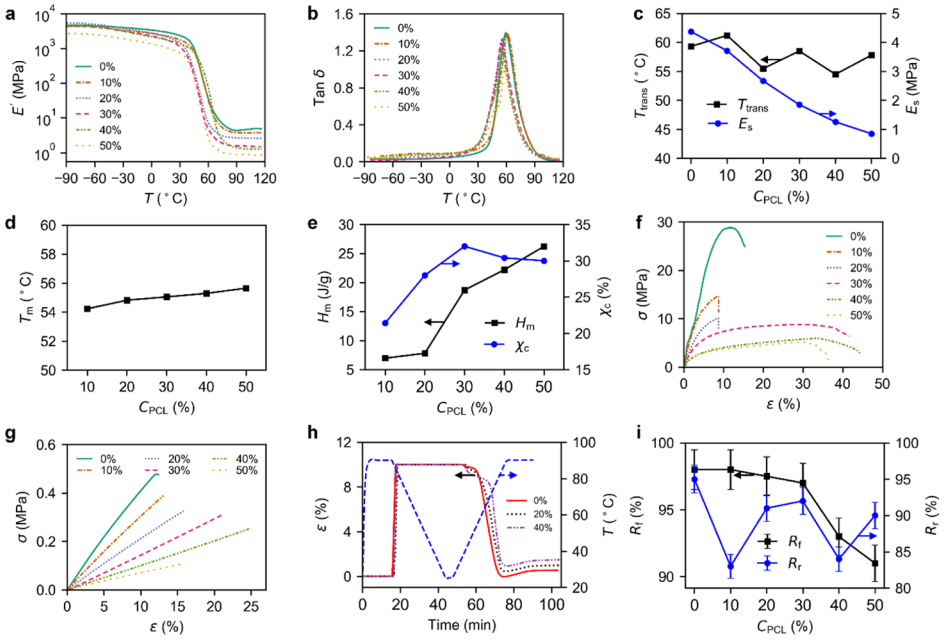

Figure 2. Thermomechanical characterization of SH-SMPs. (a) Storage modulus (E') as a function of temperature; (b) tan δ values of SH-SMPs with different PCL concentration versus temperature; (c) effect of PCL concentration (C_{PCL}) on transition temperature (T_{trans}) and soft state modulus (E_s); (d) effect of PCL concentration on melting temperature (T_m); (e) effect of PCL concentration on heat of melting (H_m) and crystallinity (χ_c); (f) uniaxial tensile testing results of SH-SMPs at room temperature (i.e., 25 °C, σ: stress, ε: strain); and (g) uniaxial tensile testing results of SH-SMPs at the soft state (i.e., 90 °C, σ: stress, ε: strain). (h) Representative SM behavior of SH-SMPs with PCL concentration at 0, 20, and 40%, respectively; and (i) summary of SM behaviors as functions of PCL concentration (R_f: shape fixity ratio and R_r: shape recovery ratio).

covalently connects the monomers and cross-linkers to solidify the liquid solution into a corresponding solid pattern. The 3D printing process proceeds by irradiating different patterned UV images onto the polymer solution layer by layer until the entire 3D structure is completed. At the high temperature, PCL is at the melt state, and the entire PCL linear chains with high polymer chain mobility penetrate into the SMP network. After cooling down the 3D printed structure to room temperature, the PCL linear chains form semicrystalline domains within the SMP network.[10]

The methacrylate-based monomer and cross-linker ensure that the SH-SMP solution has a good compatibility with the DLP-based high-resolution 3D printing. Figure 1c shows that using the SH-SMP solution, we are able to achieve a good lateral printing resolution up to 30 μm (Figure 1c(I)) and highly complex 3D geometries such as a Kelvin foam in Figure 1c(II). The BMA−PEGDMA SMP network imparts the SM effect into the 3D printed structure to realize 4D printing. As presented in Figure 1d, the thermomechanical programmed (compressed) Kelvin foam recovers into its as-printed shape upon heating at 80 °C within 5 s. More importantly, the penetrated PCL semicrystalline domains endow the self-healing ability into printed structures. The self-healing feature is shown in Figure 1e, where a broken chess piece was repaired after attaching the two separate parts at 80 °C for 5 min.

3.1. Thermomechanical Performance. As the penetration of PCL into the BMA−PEGDMA SMP system imparts self-healing ability into the SMP system, it is essential to investigate the effect of the addition of PCL on the thermomechanical behavior of the SH-SMP system. Figure 2a−c presents the DMA results of the SMP system loaded with different percentages of PCL. Figure 2a shows the variation of temperature-dependent storage modulus which corresponds to the elastic response of a tested sample. Figure 2b plots the temperature-dependent tan δ which is defined as the ratio of loss modulus (corresponding to energy dissipation) and storage modulus and used to identify the transition temperature at its peak for a thermally responsive SMP, for example, glass transition temperature for an amorphous SMP[45] and melting/crystallization temperature for a semicrystalline SMP.[46] Figure 2c presents the effect of the concentration of PCL (C_{PCL}) on the two key features of the thermomechanical behavior of the SH-SMP system: (i) the modulus at the soft-state E_s (analogues to the rubbery state for a pure amorphous SMP) and (ii) the transition temperature (T_{trans}). It is noted that the E_s decreases from 4.4 to 0.8 MPa with the increase of C_{PCL}. This is because that E_s is proportional to the cross-linking density of the SMP network, and the addition of PCL leads to the decrease in the cross-linking density, thus the decrease in E_s. In contrast, the increase of C_{PCL} has a limited effect on T_{trans} which can be explained that the glass transition temperature (T_g) of the pure BMA−PEGDMA system ($T_g \approx$ 60 °C, which was measured using the sample with C_{PCL} = 0)[8] is closed to the T_m of PCL.[47] To characterize the T_m of the SH-SMP system with different C_{PCL}, the DSC tests were performed and the results are presented in Figure S1. The T_m is identified as the endothermic peak from the heating cycle, and the heat of melting (H_m) can be calculated through integrating the endothermic peak corresponding to the enthalpy of transition. Figure 2d presents the T_m with different C_{PCL}. T_m is about 55 °C and nearly constant with different C_{PCL}, which explains the observation that C_{PCL} has a limited effect on T_{trans} of the SH-SMP system. Figure 2e shows that the H_m increases with the increase in C_{PCL} as the higher C_{PCL} leads to more crystalline domains which require more heat to melt them. In addition, we also calculate the crystallinity χ_c of PCL in the SH-SMP system with different C_{PCL} through the equation $\chi_c = H_m/(C_{PCL} \cdot H_{m100})$, where H_{m100} is the heat of

DOI: 10.1021/acsami.9b00359
ACS Appl. Mater. Interfaces 2019, 11, 10328−10336

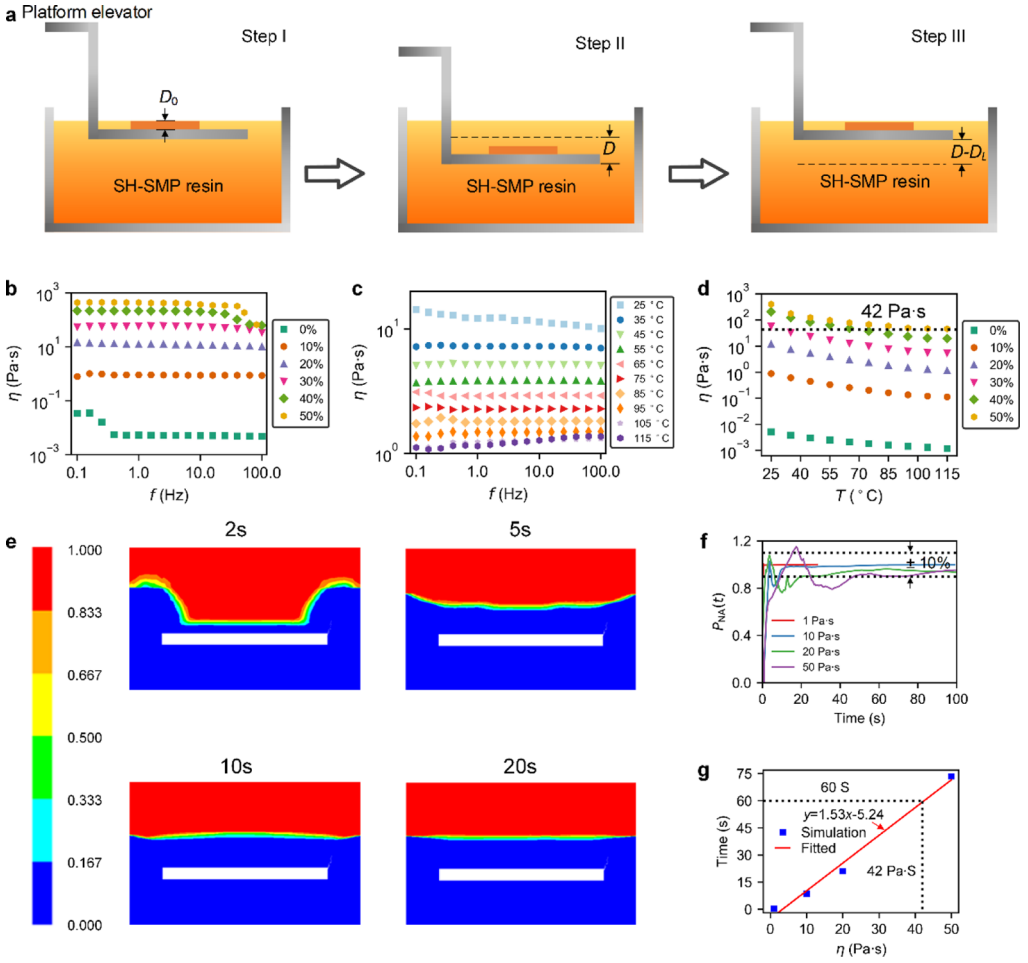

Figure 3. Effect of viscosity on the 3D printing process. (a) 3D printing process; (b) viscosity (η) of 3D printable resins with different PCL concentrations vs frequency (f); (c) viscosity of 3D printable resins with 20% PCL concentration; (d) effect of temperature on the viscosity of 3D printable resins with different PCL concentrations; (e) CFD analytical liquid state (η = 10 Pa s) at different times (red color indicates the air, and blue color indicates the liquid. The scale bar represents the volume fraction of the air); (f) normalized average pressure (P_{NA}) on the top face of the platform; and (g) time needed for the liquid to reach the steady stage as a function of viscosity.

melting of a pure PCL sample (139 J/g).[47] In Figure 2e, the χ_c slightly increases from ~20 to ~30% with the increase in C_{PCL} from 10 to 50%.

To investigate the effect of C_{PCL} on the stress−strain behavior of the SH-SMP system, we performed the uniaxial tensile tests at room temperature and high temperature (i.e., 90 °C). As shown in Figure 2f, the stiffness of the SH-SMP system at room temperature decreases with the increase in C_{PCL} because the stiffness (~100 MPa)[48] of pure semicrystalline PCL is lower than that (~300 MPa) of the pure methacrylate SMP at room temperature (the green curve in Figure 2f), but the addition of PCL also introduces the ductility of the SH-SMP system. Figure 2g shows the same effect of C_{PCL} on the stress−strain behavior of the SH-SMP system at high temperatures. It is also found that when C_{PCL} increases to 50%, the failure strains of the SH-SMP system at both room temperature and high temperature no longer increase. We further investigate the effect of C_{PCL} on the SM behavior of the SH-SMP system. As shown in Figures 2h and S2, the SH-SMP samples with different C_{PCL} were stretched by 10% at 90 °C. After cooling and unloading at room temperature, the SH-SMP samples with different C_{PCL} exhibit good shape fixity. The SH-SMP samples also demonstrate good shape recovery after heating back to 90 °C. To quantify the SM behavior, we calculate the shape fixity R_f as $R_f = \varepsilon_u/\varepsilon_m \times 100\%$, and the shape recovery ratio R_r as $R_r = (\varepsilon_u - \varepsilon_r)/\varepsilon_u \times 100\%$, where ε_m is the maximum strain before unloading, ε_u is the strain right after unloading, and ε_r is the instantaneous strain during recovery. Figure 2i shows the effect of C_{PCL} on both R_f and R_r. With the increase in C_{PCL}, the shape fixity R_f gradually decreases from 95 to 83% which is because the R_f of an SMP system is highly related to its stiffness at room temperature,[46] and the increase in C_{PCL} leads to a lower stiffness of the SMP system (Figure 2f) and therefore a lower R_f. In contrast, the shape recovery ratio R_r is not clearly influenced with the change of C_{PCL} and remains at a reasonably good level between 83 and 95% with different C_{PCL}.

3.2. Effect of Viscosity on the 3D Printing Process. We printed all the self-healing 4D printing structures on a top-down DLP-based 3D printing system.[8] As depicted in Figure 3a, after printing a structure with thickness D_0 = 1 mm (step I in Figure 3a), the printing platform moves down by D (D = 5 mm in the current 3D printing system) to allow the polymer resin to cover the printed structure (step II in Figure 3a) and then moves up by $D-D_L$ (where D_L is the layer thickness and D_L = 50 μm) for printing the following layer (step III in Figure 3a). After moving down by D, the printing platform needs to stay stationary and wait until the polymer solution ceases the

DOI: 10.1021/acsami.9b00359
ACS Appl. Mater. Interfaces 2019, 11, 10328−10336

fluctuation. The duration of the waiting time is proportional to the viscosity of the polymer solution, and it is not practical to use a highly viscous polymer solution which requires to wait for more than 1 min for each layer. Therefore, it is critical to systematically investigate the rheological behavior of the SH-SMP solution with different PCL concentrations. Figure 3b plots the viscosity of the SH-SMP solutions as a function of frequency at room temperature. The viscosity of all solutions shows no apparent difference at the testing frequency range (from 0.1 to 100 Hz) and thus can be regarded as the Newtonian fluid. The increase in C_{PCL} from 0 to 50% results in the raise of viscosity at room temperature from 0.01 to 400 Pa s. We further investigated the effect of temperature on the viscosity of the SH-SMP system. Figure 3c shows the representative results of the SH-SMP solution with 20% PCL. The solution behaves as a Newtonian fluid at different temperatures, and the temperature elevation from 25 to 75 °C reduces the viscosity from ∼10 to ∼2 Pa s. The investigations on the temperature effects for the SH-SMP solutions with different C_{PCL} are presented in Figure S3 and summarized in Figure 3d by showing the viscosities at a frequency of 10 Hz. With the increase in temperature, the viscosity of all of the testing SH-SMP solutions decreases by about 1 order of magnitude, which shows the possibility to print 4D printing structures with high PCL concentration SH-SMP solutions by increasing the temperature.

To quantitatively investigate the effect of viscosity on the printing process, we simulated the fluid−structure interaction during the printing process using the commercial CFD software package ANSYS FLUENT 17.2 (ANSYS, Inc., USA). Figure 3e presents the representative simulation result during the waiting process. It takes about 10 s to cease the fluctuation in the case that the printing platform moves down by 5 mm in the printing solution with a viscosity of 10 Pa s. The details about the simulation process are provided in Supporting Information part 4. The surface tension and contact angle needed in the CFD calculation were measured using the pendant drop and the curve fitting methods, respectively, and are provided in Supporting Information part 5. To determine the duration of waiting time, we set the criterion that the normalized average pressure $P_{NA}(t)$ on the top surface of the printing solution must satisfy the following condition: $P_\infty - \Delta P < P_{NA}(t) < P_\infty + \Delta P$. Here, P_∞ is the ultimate pressure of a low viscous fluid (1 Pa s) after waiting for a sufficient long flow time (1000 s) and ΔP is the admissible tolerance. We set ΔP to be $0.1P_\infty$ after comparing simulation with the experiment. Figure 3f shows the variation of $P_{NA}(t)$ of the printing solution with different viscosities. Based on this, Figure 3g plots the relation between the waiting time and viscosity of the polymer solution which shows strong linear relationship and suggests that the viscosity of the printing solution should be reduced to less than 42 Pa s to ensure that the waiting time is within 1 min. According to the viscosity−temperature relation in Figure 3d, the SH-SMP solutions with 30, 40, and 50% of PCL need to be heated to 40, 70, and 100 °C, respectively, to reduce the viscosity to less than 42 Pa s.

3.3. Self-Healing Characterization. We endow the self-sealing ability into the 4D printing SMP system by using PCL as a self-healing agent.[49,50] The self-healing mechanism is illustrated in Figure 4a. At room temperature, two separated sample strips are placed in contact (Figure 4a(I)). After heating to a temperature higher than T_m of PCL, the PCL

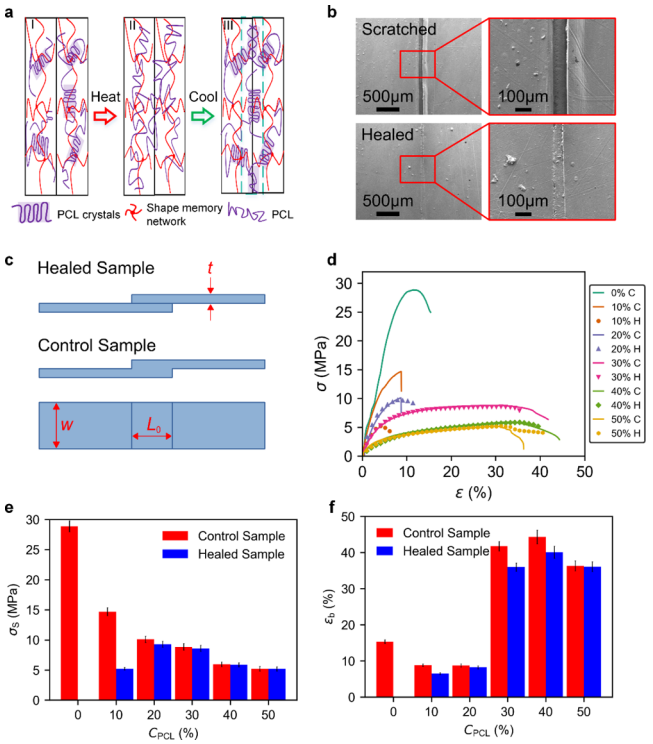

Figure 4. Self-healing behavior of SH-SMPs. (a) Illustrations of the self-healing mechanism. (b) SEM micrographs of scratched and healed surface at different scales. (c) Schematic illustrations of lap-shear testing samples. (d) Strain−stress curves of healed and control samples with different PCL concentrations (C represents control sample and H represents healed sample). (e) Effect of PCL concentration on the strength σ_S. (f) Effect of PCL concentration on the strain at break ε_b.

crystalline domains melt and the PCL linear chains diffuse through the boundary between two separated sample strips (Figure 4a(II)). When cooling down to room temperature, the PCL linear chains form crystalline domains. Some crystalline domains are across the boundary between separate strips and bond them together (Figure 4a(III)). We demonstrate the self-healing ability in Figure 4b, where we first generated a crack region with a width of ∼100 μm on the surface of a printed sample with 20% PCL by scratching the sample with a blade; after heating at 80 °C for 20 min, the scratch nearly disappears indicating that the printed sample possesses a good self-healing ability. We carried out the lap-shear experiments to quantitatively investigate the self-healing ability of the SH-SMP system. As shown in Figure 4c, we prepared the testing sample by bonding two printed rectangular samples (width w × thickness t = 10 mm × 1.5 mm) with the shear area ($L_0 \times w$) of 7 mm × 10 mm at 80 °C for 30 min. The control specimens with the same shape and dimensions were prepared by 3D printing. Uniaxial tensile tests were conducted on both healed and control samples at room temperature to evaluate the self-healing properties. Details about the sample preparation and the lap-shear experiments can be found in 2.8.

Figure 4d compares the strain−stress curves of control and repaired samples with different C_{PCL}. Figure 4e summarizes the relation between C_{PCL} and strength σ_S of the tested samples. If C_{PCL} is higher than 20%, the repaired sample can recover nearly 100% of the strength of the control sample. Figure 4f shows the same trend to the relation between C_{PCL} and strain at break ε_b, indicating that the repaired sample can recover

DOI: 10.1021/acsami.9b00359
ACS Appl. Mater. Interfaces 2019, 11, 10328−10336

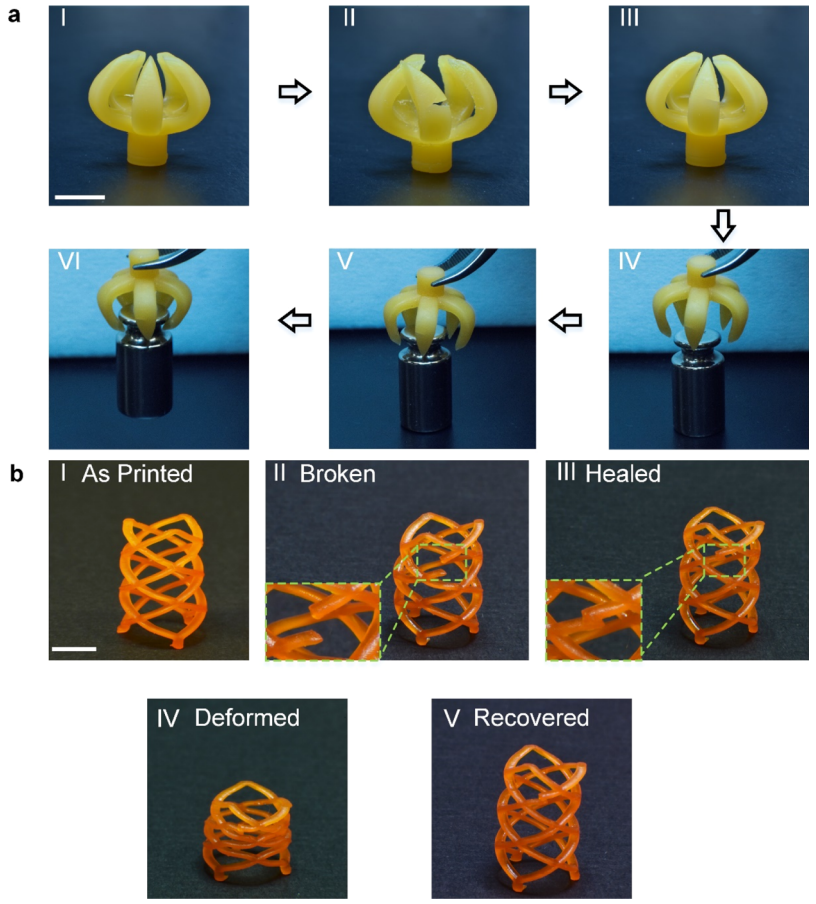

Figure 5. Application demonstrations of SH-SMPs. (a) 3D printed gripper (I) as-printed gripper. (II) Cut gripper. (III) Healed gripper. (IV–VI) Grabbing process. (b) 3D printed stent (I) as-printed. (II) Broken. (III) Healed. (IV) Deformed. (V) Recovered. (Scale bars: 4 mm).

nearly 100% of the strain at break of the control sample when C_{PCL} is 20% or higher.

3.4. Application. Owing to the ability to repair damaged 3D printed objects and restore their original functionalities, the proposed 3D printable SH-SMPs have the potential application in areas such as soft robotics, flexible electronics, and biomedical devices. In Figure 5a, we presented the printing of a 3D printed SH-SMPs gripper that has the potential to function as actuated grippers[51,52] and drug-delivery devices.[43,53] As shown in Figure 5a, an as-printed closed gripper from SH-SMPs (Figure 5a(I)) was partially cut (Figure 5a(II)) and then healed at 80 °C for 5 min (Figure 5a(III)). By heating at 80 °C, the healed gripper can be deformed to the opened temporary shape. Once opened, the structure was cooled down at room temperature to fix the temporary shape (Figure 5a(IV)). Upon reheating the opened gripper at $T > T_{trans}$, the claws recovered to the printed shape, and the gripper was able to grab a weight of 10 g (Figure 5a(V,VI)). Figure 5b shows another notable potential application of our SH-SMPs system cardiovascular stent. The cardiovascular stent is widely used to treat angiocardiopathy. Traditional efforts to fabricate SM stent mainly focused on conventional fabrication methods.[42,54,55] Here, we printed a stent with both SM and self-healing effects. Figure 5b(I) showed the intact stent that was 3D printed by our SH-SMP materials. The stent may break because of the external force. As shown in Figure 5b(II), the stent was cut by a knife and one piece was broken. Then, the stent was heated to 80 °C and the broken parts were held together by a tweezer for 10 s. Consequently, the broken parts were reconnected, as shown in Figure 5b(III). Then, the healed stent was programmed to a temporary shape, as shown in Figure 5b(IV). Upon heating, the healed stent can recover to its permanent shape again, as shown in Figure 5b(V).

4. CONCLUSIONS

In summary, we report an approach to develop a double-network SH-SMP system for high-resolution self-healing 4D printing. The SH-SMP-based 4D printing with high resolutions (up to 30 μm) and geometric complexity was successfully achieved, and the printed objects show remarkable SM and self-healing properties. The rheological behavior of the SH-SMP material was systematically studied both experimentally and theoretically to investigate the printability of the resins. Damaged 3D printed structures from such SH-SMPs can be repaired and can recover their SM functionality, which extend their lifespan.

■ ASSOCIATED CONTENT

Supporting Information

The Supporting Information is available free of charge on the ACS Publications website at DOI: 10.1021/acsami.9b00359.

Relation between temperature and heat flow at different PCL concentrations; SM behavior of SH-SMPs with PCL concentration at 10, 30, and 50%; viscosity of 3D printable resins with different PCL concentrations as a function of frequency at different temperatures; CFD

DOI: 10.1021/acsami.9b00359
ACS Appl. Mater. Interfaces 2019, 11, 10328–10336

simulation; surface tension and contact angle measurement; and DLP process parameters (PDF)

AUTHOR INFORMATION

Corresponding Author

*E-mail: ge_qi@sutd.edu.sg.

ORCID

Qi Ge: 0000-0002-8666-8532

Author Contributions

B.Z. and W.Z. contributed equally. The manuscript was written through contributions of all authors. All authors have given approval to the final version of the manuscript.

Notes

The authors declare no competing financial interest.

ACKNOWLEDGMENTS

B.Z., W.Z., and Q.G. gratefully acknowledge the support from the Agency for Science, Technology and Research (A*STAR) Public Sector Funding (PSF) (Project number 1521200086). Y.-F.Z. and Q.G. acknowledge the support from the SUTD Digital Manufacturing and Design Center (DManD). Q.G. acknowledges the SUTD Start-up Research Grant. B.Z. acknowledges Northwestern Polytechnical University (NPU) Start-up Research Grant. W.Z. is grateful for his SUTD President's Graduate Fellowship. Z.L. acknowledges RIE2020 AME Programmatic Grant (A18A1b0045) funded by A*STAR-SERC, Singapore. The authors also thank Prof. Ping Wu and Dr. Anupama Sargur Ranganath from SUTD for the technical assistance.

REFERENCES

(1) Ge, Q.; Qi, H. J.; Dunn, M. L. Active Materials by Four-Dimension Printing. *Appl. Phys. Lett.* **2013**, *103*, 131901.

(2) Ge, Q.; Dunn, C. K.; Qi, H. J.; Dunn, M. L. Active Origami by 4D Printing. *Smart Mater. Struct.* **2014**, *23*, 094007.

(3) Raviv, D.; Zhao, W.; McKnelly, C.; Papadopoulou, A.; Kadambi, A.; Shi, B.; Hirsch, S.; Dikovsky, D.; Zyracki, M.; Olguin, C. Active Printed Materials for Complex Self-Evolving Deformations. *Sci. Rep.* **2014**, *4*, 7422.

(4) Sydney Gladman, A.; Matsumoto, E. A.; Nuzzo, R. G.; Mahadevan, L.; Lewis, J. A. Biomimetic 4D printing. *Nat Mater* **2016**, *15*, 413−8.

(5) Tibbits, S. 4D Printing: Multi-Material Shape Change. *Architect. Des.* **2014**, *84*, 116−121.

(6) Truby, R. L.; Lewis, J. A. Printing Soft Matter in Three Dimensions. *Nature* **2016**, *540*, 371−378.

(7) Patel, D. K.; Sakhaei, A. H.; Layani, M.; Zhang, B.; Ge, Q.; Magdassi, S. Highly Stretchable and UV Curable Elastomers for Digital Light Processing based 3D Printing. *Adv. Mater.* **2017**, *29*, 1606000.

(8) Ge, Q.; Sakhaei, A. H.; Lee, H.; Dunn, C. K.; Fang, N. X.; Dunn, M. L. Multimaterial 4D Printing with Tailorable Shape Memory Polymers. *Sci. Rep.* **2016**, *6*, 31110.

(9) Zarek, M.; Mansour, N.; Shapira, S.; Cohn, D. 4D Printing of Shape Memory-Based Personalized Endoluminal Medical Devices. *Macromol. Rapid Commun.* **2016**, *38*, 1600628.

(10) Zarek, M.; Layani, M.; Cooperstein, I.; Sachyani, E.; Cohn, D.; Magdassi, S. 3D Printing of Shape Memory Polymers for Flexible Electronic Devices. *Adv. Mater.* **2015**, *28*, 4449−4454.

(11) Huang, L.; Jiang, R.; Wu, J.; Song, J.; Bai, H.; Li, B.; Zhao, Q.; Xie, T. Ultrafast Digital Printing toward 4D Shape Changing Materials. *Adv. Mater.* **2016**, *29*, 1605390.

(12) Miao, S.; Castro, N.; Nowicki, M.; Xia, L.; Cui, H.; Zhou, X.; Zhu, W.; Lee, S.-j.; Sarkar, K.; Vozzi, G.; Tabata, Y.; Fisher, J.; Zhang, L. G. 4D Printing of Polymeric Materials for Tissue and Organ Regeneration. *Mater. Today* **2017**, *20*, 577−591.

(13) Momeni, F.; Mehdi Hassani N, S. M.; Liu, X.; Ni, J. A Review of 4D Printing. *Mater. Des.* **2017**, *122*, 42−79.

(14) Khoo, Z. X.; Teoh, J. E. M.; Liu, Y.; Chua, C. K.; Yang, S.; An, J.; Leong, K. F.; Yeong, W. Y. 3D Printing of Smart Materials: A Review on Recent Progresses in 4D Printing. *Virtual Phys. Prototyp.* **2015**, *10*, 103−122.

(15) Guo, J.; Zhang, R.; Zhang, L.; Cao, X. 4D Printing of Robust Hydrogels Consisted of Agarose Nanofibers and Polyacrylamide. *ACS Macro Lett.* **2018**, *7*, 442−446.

(16) Bodaghi, M.; Damanpack, A. R.; Liao, W. H. Triple Shape Memory Polymers by 4D Printing. *Smart Mater. Struct.* **2018**, *27*, 065010.

(17) Kuang, X.; Chen, K.; Dunn, C. K.; Wu, J.; Li, V. C. F.; Qi, H. J. 3D Printing of Highly Stretchable, Shape-Memory, and Self-Healing Elastomer toward Novel 4D Printing. *ACS Appl. Mater. Interfaces* **2018**, *10*, 7381−7388.

(18) Bakarich, S. E.; Gorkin, R.; Panhuis, M. i. h.; Spinks, G. M. 4D Printing with Mechanically Robust, Thermally Actuating Hydrogels. *Macromol. Rapid Commun.* **2015**, *36*, 1211−1217.

(19) Nadgorny, M.; Xiao, Z.; Chen, C.; Connal, L. A. Three-Dimensional Printing of pH-Responsive and Functional Polymers on an Affordable Desktop Printer. *ACS Appl. Mater. Interfaces* **2016**, *8*, 28946−28954.

(20) Naficy, S.; Gately, R.; Gorkin, R., III; Xin, H.; Spinks, G. M. 4D Printing of Reversible Shape Morphing Hydrogel Structures. *Macromol. Mater. Eng.* **2016**, *302*, 1600212.

(21) Kirillova, A.; Maxson, R.; Stoychev, G.; Gomillion, C. T.; Ionov, L. 4D Biofabrication Using Shape-Morphing Hydrogels. *Adv. Mater.* **2017**, *29*, 1703443.

(22) Zhang, Q.; Yan, D.; Zhang, K.; Hu, G. Pattern Transformation of Heat-shrinkable Polymer by Three-Dimensional (3D) Printing Technique. *Sci. Rep.* **2015**, *5*, 8936.

(23) Mao, Y.; Ding, Z.; Yuan, C.; Ai, S.; Isakov, M.; Wu, J.; Wang, T.; Dunn, M. L.; Qi, H. J. 3D Printed Reversible Shape Changing Components with Stimuli Responsive Materials. *Sci. Rep.* **2016**, *6*, 24761.

(24) Lendlein, A.; Kelch, S. Shape-Memory Polymers. *Angew. Chem., Int. Ed.* **2002**, *41*, 2034−2057.

(25) Xie, T. Tunable Polymer Multi-Shape Memory Effect. *Nature* **2010**, *464*, 267−270.

(26) Lendlein, A.; Jiang, H.; Jünger, O.; Langer, R. Light-Induced Shape-Memory Polymers. *Nature* **2005**, *434*, 879−882.

(27) Long, K. N.; Scott, T. F.; Jerry Qi, H.; Bowman, C. N.; Dunn, M. L. Photomechanics of Light-Activated Polymers. *J. Mech. Phys. Solids* **2009**, *57*, 1103−1121.

(28) Ryu, J.; D'Amato, M.; Cui, X.; Long, K. N.; Jerry Qi, H.; Dunn, M. L. Photo-origami-Bending and folding polymers with light. *Appl. Phys. Lett.* **2012**, *100*, 161908.

(29) Keplinger, C.; Sun, J.-Y.; Foo, C. C.; Rothemund, P.; Whitesides, G. M.; Suo, Z. Stretchable, Transparent, Ionic Conductors. *Science* **2013**, *341*, 984−987.

(30) Wang, Q.; Gossweiler, G. R.; Craig, S. L.; Zhao, X. Cephalopod-Inspired Design of Electro-Mechano-chemically Responsive Elastomers for on-Demand Fluorescent Patterning. *Nat. Commun.* **2014**, *5*, 4899.

(31) Castro, F.; Westbrook, K. K.; Long, K. N.; Shandas, R.; Qi, H. J. Effects of Thermal Rates on the Thermomechanical Behaviors of Amorphous Shape Memory Polymers. *Mech. Time-Depend. Mater.* **2010**, *14*, 219−241.

(32) Yu, K.; Ge, Q.; Qi, H. J. Reduced Time as a Unified Parameter Eetermining Fixity and Free Recovery of Shape Memory Polymers. *Nat. Commun.* **2014**, *5*, 3066.

(33) Ding, Z.; Yuan, C.; Peng, X.; Wang, T.; Qi, H. J.; Dunn, M. L. Direct 4D Printing via Active Composite Materials. *Sci. Adv.* **2017**, *3*, No. e1602890.

(34) Tumbleston, J. R.; Shirvanyants, D.; Ermoshkin, N.; Janusziewicz, R.; Johnson, A. R.; Kelly, D.; Chen, K.; Pinschmidt,

DOI: 10.1021/acsami.9b00359
ACS Appl. Mater. Interfaces 2019, 11, 10328−10336

R.; Rolland, J. P.; Ermoshkin, A.; Samulski, E. T.; DeSimone, J. M. Continuous Liquid Interface Production of 3D Objects. *Science* **2015**, *347*, 1349−1352.
(35) Zhang, B.; Li, S.; Hingorani, H.; Serjouei, A.; Larush, L.; Pawar, A. A.; Goh, W. H.; Sakhaei, A. H.; Hashimoto, M.; Kowsari, K.; Magdassi, S.; Ge, Q. Highly Stretchable Hydrogels for UV Curing based High-Resolution Multimaterial 3D Printing. *J. Mater. Chem. B* **2018**, *6*, 3246−3253.
(36) Invernizzi, M.; Turri, S.; Levi, M.; Suriano, R. 4D Printed Thermally Activated Self-Healing and Shape Memory Polycaprolactone-based Polymers. *Eur. Polym. J.* **2018**, *101*, 169−176.
(37) Rus, D.; Tolley, M. T. Design, Fabrication and Control of Soft Robots. *Nature* **2015**, *521*, 467−475.
(38) Bartlett, N. W.; Tolley, M. T.; Overvelde, J. T. B.; Weaver, J. C.; Mosadegh, B.; Bertoldi, K.; Whitesides, G. M.; Wood, R. J. A 3D-Printed, Functionally Graded Soft Robot Powered by Combustion. *Science* **2015**, *349*, 161−165.
(39) Wehner, M.; Truby, R. L.; Fitzgerald, D. J.; Mosadegh, B.; Whitesides, G. M.; Lewis, J. A.; Wood, R. J. An Integrated Design and Fabrication Strategy for Entirely Soft, Autonomous Robots. *Nature* **2016**, *536*, 451−455.
(40) Gall, K.; Mikulas, M.; Munshi, N. A.; Beavers, F.; Tupper, M. Carbon Fiber Reinforced Shape Memory Polymer Composites. *J. Intell. Mater. Syst. Struct.* **2000**, *11*, 877−886.
(41) Lan, X.; Liu, Y.; Lv, H.; Wang, X.; Leng, J.; Du, S. Fiber Reinforced Shape-Memory Polymer Composite and its Application in a Deployable Hinge. *Smart Mater. Struct.* **2009**, *18*, 024002.
(42) Yakacki, C. M.; Shandas, R.; Lanning, C.; Rech, B.; Eckstein, A.; Gall, K. Unconstrained Recovery Characterization of Shape-Memory Polymer Networks for Cardiovascular Applications. *Biomaterials* **2007**, *28*, 2255−2263.
(43) Breger, J. C.; Yoon, C.; Xiao, R.; Kwag, H. R.; Wang, M. O.; Fisher, J. P.; Nguyen, T. D.; Gracias, D. H. Self-Folding Thermo-Magnetically Responsive Soft Microgrippers. *ACS Appl. Mater. Interfaces* **2015**, *7*, 3398−3405.
(44) Montarnal, D. *Use of Reversible Covalent and Non-covalent Bonds in New Recyclable and Reprocessable Polymer Materials*; Université Pierre et Marie Curie-Paris VI, 2011.
(45) Ge, Q.; Yu, K.; Ding, Y.; Jerry Qi, H. Prediction of Temperature-Dependent Free Recovery Behaviors of Amorphous Shape Memory Polymers. *Soft Matter* **2012**, *8*, 11098−11105.
(46) Ge, Q.; Luo, X.; Rodriguez, E. D.; Zhang, X.; Mather, P. T.; Dunn, M. L.; Qi, H. J. Thermomechanical Behavior of Shape Memory Elastomeric Composites. *J. Mech. Phys. Solids* **2012**, *60*, 67−83.
(47) Woodruff, M. A.; Hutmacher, D. W. The return of a forgotten polymer-Polycaprolactone in the 21st century. *Prog. Polym. Sci.* **2010**, *35*, 1217−1256.
(48) Ge, Q.; Serjouei, A.; Qi, H. J.; Dunn, M. L. Thermomechanics of Printed Anisotropic Shape Memory Elastomeric Composites. *Int. J. Solids Struct.* **2016**, *102*−*103*, 186−199.
(49) Rodriguez, E. D.; Luo, X.; Mather, P. T. Linear/Network Poly(ε-caprolactone) Blends Exhibiting Shape Memory Assisted Self-Healing (SMASH). *ACS Appl. Mater. Interfaces* **2011**, *3*, 152−161.
(50) Luo, X.; Mather, P. T. Shape Memory Assisted Self-healing Coating. *ACS Macro Lett.* **2013**, *2*, 152−156.
(51) Mølhave, K.; Hansen, O. Electro-Thermally Actuated Micro-grippers with Integrated Force-Feedback. *J. Micromech. Microeng.* **2005**, *15*, 1265.
(52) Zhang, Y.-F.; Zhang, N.; Hingorani, H.; Ding, N.; Wang, D.; Yuan, C.; Zhang, B.; Gu, G.; Ge, Q. Fast-Response, Stiffness-Tunable Soft Actuator by Hybrid Multimaterial 3D Printing. *Adv. Funct. Mater.* **2019**, 1806698.
(53) Malachowski, K.; Breger, J.; Kwag, H. R.; Wang, M. O.; Fisher, J. P.; Selaru, F. M.; Gracias, D. H. Stimuli-Responsive Theragrippers for Chemomechanical Controlled Release. *Angew. Chem., Int. Ed.* **2014**, *53*, 8045−8049.
(54) Wache, H. M.; Tartakowska, D. J.; Hentrich, A.; Wagner, M. H. Development of a Polymer Stent with Shape Memory Effect as a Drug Delivery System. *J. Mater. Sci.: Mater. Med.* **2003**, *14*, 109−112.
(55) Baer, G. M.; Small, W.; Wilson, T. S.; Benett, W. J.; Matthews, D. L.; Hartman, J.; Maitland, D. J. Fabrication and in Vitro Deployment of a Laser-Activated Shape Memory Polymer Vascular Stent. *Biomed. Eng. Online* **2007**, *6*, 43.

DOI: 10.1021/acsami.9b00359
ACS Appl. Mater. Interfaces 2019, 11, 10328−10336